AIAA JOURNAL
Vol. 31, No. 12, December 1993

Model for Rotor Tip Vortex-Airframe Interaction, Part 2: Comparison with Experiment

H. Affes* and A. T. Conlisk†
Ohio State University, Columbus, Ohio 43210
and
J. M. Kim‡ and N. M. Komerath§
Georgia Institute of Technology, Atlanta, Georgia 30332

The interaction between a vortex and a solid boundary involves the development of a variety of length and time scales, some of which are due to very strong viscous effects. Prediction of these phenomena from first principles would remove a major obstacle in the computation of flows around rotorcraft. In Part 1 of this work,[2] analytical and computational tools to advance the tip vortex in time and compute the surface pressure are presented for a vortex tube approaching an infinite circular cylinder. In this paper, quantitative comparisons are made with experimental results for a rotor tip vortex approaching a cylindrical airframe with a hemispherical leading edge. Unsteady velocity, surface pressure, and vortex trajectory data are used to define the initial conditions and perform the comparisons. The results are in substantial agreement before the impact of the vortex on the airframe.

Introduction

COMPUTATION of the time-varying flowfield around an entire rotorcraft poses severe challenges. Several highly nonlinear interactions occur,[1] so that rotorcraft performance cannot be predicted by a simple superposition of component characteristics. Several unexpected problems can also emerge during prototype testing. Research over the past decade has shown that the dominant features of the interaction between a rotor wake and an airframe can be predicted using a potential flow model of the entire rotor wake, with two major exceptions: the detailed interaction of the tip vortex with the airframe surface and the interaction of the wake with regions of separated flow on the complicated airframe shape. In this paper we present a systematic approach to the first of these problems.

In Part 1 of this work,[2] a combined analytical and computational method was presented to describe the interaction between a single vortex and an infinite circular cylinder for the time regime before vortex impact on the airframe. In this paper we present detailed comparisons between experimental and analytical/computational results for the interaction of a single vortex tube with an airframe. This vortex-cylinder configuration is a simplified model for the interaction produced when the rotor tip vortex impinges on the airframe of a helicopter. Previous work by the authors has given a preliminary experimental view of the interaction between a tip vortex and the airframe[3,4] and initial qualitative analytical/computational comparisons have been encouraging.[5] This paper presents quantitative comparisons of the experimental and analytical/computational results based on the methods developed in Part 1. Comparisons between theory and experiment will be made in the areas of vortex position and pressure distribution on the airframe before vortex impact; in addition, the characteristics of the initial stages of the impact of the vortex filament with the cylinder will be discussed.

Received May 29, 1992; revision received March 15, 1993; accepted for publication March 15, 1993.

*Graduate Research Assistant, Department of Mechanical Engineering.
†Associate Professor, Department of Mechanical Engineering. Member AIAA.
‡Graduate Research Assistant, School of Aerospace Engineering.
§Associate Professor, School of Aerospace Engineering. Senior Member AIAA.

The experimental results presented in this paper are an extension of those of Liou et al.[3] (see also Brand et al.[4] and Brand[6]). They used laser Doppler velocimetry to measure the velocity in the vicinity of the filament and obtained results for the pressure on the surface of the cylinder under the impinging vortex. The physical situation is depicted in Fig. 1. In addition, they were able to map the vortex position as a function of time, including the period during which a portion of the vortex impacts the cylinder. Bi and Leishman[7,8] and Leishman and Bi[9] also reported on the interaction of the tip vortex filament with an airframe. The work of Lorber and Egolf[10] (and some additional references therein) represented a large-scale computational effort to compute the entire wake flow and its interaction with a simulated helicopter fuselage; they also presented results for the airframe geometry of Refs. 3, 4, and 6. They used a prescribed wake geometry, with the vortex trajectory bent around the airframe to enable the computation to continue beyond the point when the vortex first reaches the airframe surface. They were able to capture the effect of blade passage and tip vortex qualitatively. In general, quantitative agreement is difficult because the accuracy and resolution of the tip vortex effect is severely limited by the grid and wake model used since the influence of the tip vortex is confined to a narrow band under the vortex. (See Figs. 3, 10, and 16 of that work.) The work of Mavris et al.[11] was mainly concerned with the modeling of the mean pressure on the airframe although they were also able to capture the unsteady blade passage effect using a simple two-dimensional airfoil (in a uniform freestream) model.

As mentioned in Part 1,[2] Quakenbush and Bliss[12] have developed a "fat core" model based on the classical panel method to prevent the development of singularities when the vortex comes too close to the surface control panel points. Their objective is to reduce the large amplitude of the induced velocity as the vortex collides with the surface so that the numerical algorithm will not fail on collision. Komerath et al.[13] succeeded in accurately modeling the periodic surface pressure fluctuations on the top of the airframe using a large-scale rotor wake code except during the time regime of significant vortex-surface interaction. Nominally, this time period runs from precollision through the postcollision phases. In this paper we address the characteristics of the approach vortex trajectory and the precollision phenomena on the surface. In the course of this work no free constants will be employed to better match the experimental data, and thus the value of the present work is that it is predictive in character.

It is useful at this point to discuss the factors that influence the pressure distribution on the airframe; for definiteness, and since

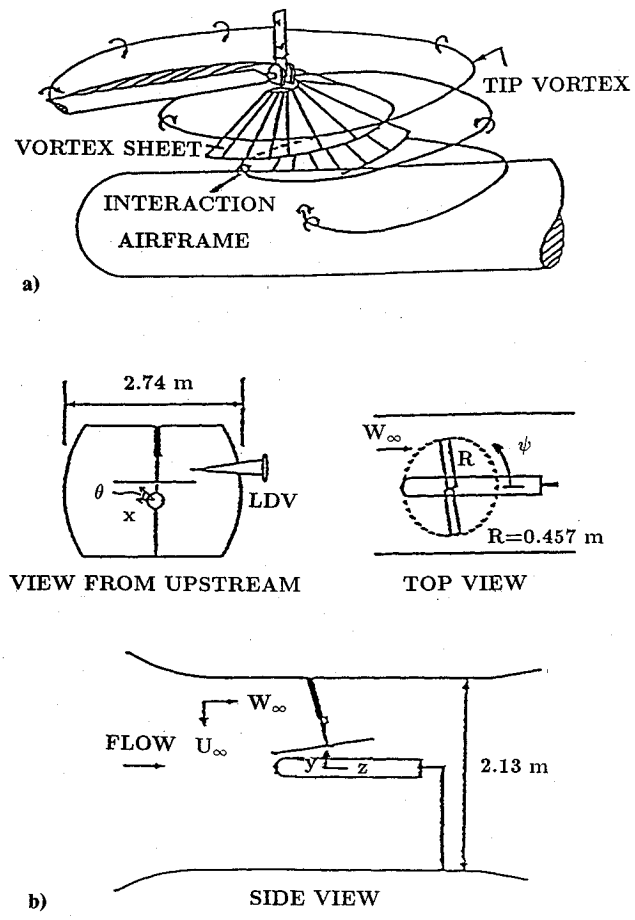

Fig. 1 a) Wake of a single-bladed rotor in low-speed forward flight and b) experimental configuration and coordinate system.

the effects are most felt on the top of the airframe, we confine the discussion to this portion of the airframe. The following comments apply to the case of advance ratio $\mu = 0.1$, although similar comments apply to other advance ratios. A complete presentation of the experimental results over an entire period for the case of $\mu = 0.075$ is given in Refs. 4 and 6.

Figure 2 shows phase-resolved pressure data acquired along the top of the airframe during the vortex interaction. Here the pressure is normalized by $\frac{1}{2}\rho W_\infty^2$ where W_∞ is the mean velocity along the generators of the cylinder. In Fig. 2, the sharp peaks occurring at rotor phase $\psi = 0$ and 180 deg are due to the passage of the rotor over the airframe. These diminish downstream, reflecting the decrease of rotor tangential velocity toward the rotor hub. The oblique features on the figure are the pressure traces of the vortex-surface interaction. The deep valley in the pressure beginning about 10 deg after blade passage is due primarily to the tip vortex impinging on the surface; the amplitude of this valley reaches a maximum near the time of vortex impact with the cylinder, and this amplitude decreases as the vortex moves downstream and below the airframe. The effect of tip filament appears to be significant from about $\psi \sim 10$ to 60 deg when the portion of the tip filament impacts the top of the airframe. From about $\psi = 60$ to 162 deg the effect of the balance of the rotor wake is significant; this is reflected in the presence of the valley that appears at about $\psi = 40$ and 220 deg and diverges away from the tip trace. The blade passage effect again begins to be felt about $\psi = 150$ deg and reaches a maximum at about $\psi = 180$ deg and the cycle repeats again. The present work is concerned with the influence of the tip filament on the airframe; hence, the time period of interest is from approximately $\psi \sim 10$ to 60 deg. Of course, precise values of ψ depend on the advance ratio and other parameters.

The goal of the present work is to determine whether the present analytical and computational techniques can adequately predict the motion of the tip vortex filament near the airframe and the induced pressure distribution. The parameters of interest correspond to advance ratios of $\mu = 0.075$ and 0.1; other experimental parameters are as in Brand et al.[4] and Brand.[6] The plan of the paper is as follows. The experimental apparatus and methodology are discussed first; the analytical/numerical techniques are then discussed briefly; details of these techniques are presented by Affes and Conlisk[2] in Part 1 of this work. Some computational aspects involved in modeling the complex flowfield around the airframe are then discussed. Detailed results for the vortex trajectory and the pressure distribution on the airframe are then presented; this section is followed by the summary and conclusions, which include a discussion of the initial stages of the vortex impact problem.

Experimental Methods

All of the experimental measurements were performed in the John J. Harper wind tunnel at the Georgia Institute of Technology. The experimental configuration is shown in Fig. 1. The vortex is generated at the tip of each of the two, constant-chord, untwisted NACA 0015 blades of a rotor turning at 2100 rpm; thus the wake geometry is periodic with period π. The radius of the rotor is 0.457 m, and the airframe model is a cylinder of radius 0.067 m. The rotor is tilted at an angle of 6 deg to the vertical. Complete details of the design of the experimental configuration have been presented in previous work.[3,4,6] Three distinct sets of experimental data are of interest in the present work: tip vortex position, mean pressure on the surface of the airframe, and unsteady surface pressure data. We discuss each in some detail in what follows.

The tip vortex filament position at each time step was determined by strobed laser sheet visualization. The flow was uniformly seeded with atomized mineral oil and the vortex cores were thus seen as regions devoid of light-scattering material; videography was employed to quantify the trajectories. A pulsed copper vapor laser was employed to acquire images of the vortex core with 25 ns temporal resolution to see the changes in shape as the vortex approaches the airframe. To capture the image of the moving vortex core, an argon ion laser sheet was strobed near the fundamental frequency of the rotor that is 70 Hz; data were taken at successive values of the azimuthal angle ψ, which is essentially a timelike variable. Since the rotor consists of two blades, two vortex filaments 180 deg apart in age exist simultaneously; for example, the tip vortex filament present at 210 deg coexists with the fil-

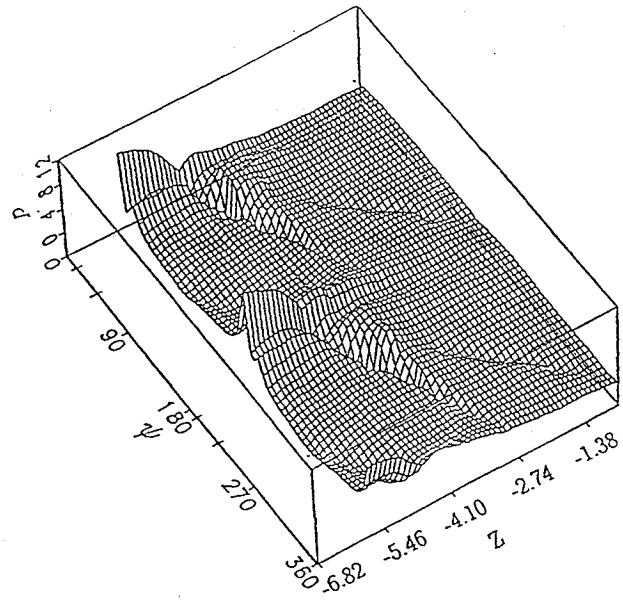

Fig. 2 Three-dimensional perspective view of the experimental unsteady pressure variation along the airframe surface. The advance ratio is $\mu = 0.1$. Note the blade passage effect near $\psi = 0$, 180, and 360 deg. The regime of interest in the present modeling effort is indicated by the additional tick marks.

ament present at 390 deg that was shed from the previous blade. Once the data for the vortex trajectory were taken at a given value of ψ, the videotape was reviewed and positions of the vortex core, visible as dark spots, were plotted on the image of a square grid placed at the measuring plane. The rotor azimuth was determined as follows: since the strobing frequency is not equal to the rotor frequency, the rotor azimuth changes slowly from frame to frame. By counting the time taken for the azimuth to describe 360 deg, the rotor azimuth is calculated. The accuracy here is of the order of 3 deg, limited by the 0.1-s least count of the camera clock.

The error in the measurement of the vortex positions is estimated to be approximately 15 mm, which is about twice the average vortex core radius over the regime $\psi = 0$ to 60 deg, which corresponds approximately to the time of impact for $\mu = 0.1$. Here ψ is measured from the beginning of a period and μ is the advance ratio $\mu = W_\infty/R\Omega$ where W_∞ is the axial mean flow velocity, R is the rotor radius, and Ω is the angular velocity of the rotor. The results of the measurements of the vortex trajectory are used to define the initial conditions for the numerical calculations.

The mean surface pressure was obtained by the use of a single array of static pressure taps oriented along the airframe at specified locations. Since the model airframe is axisymmetric, the tap row can be positioned by rotating about its axis of symmetry. A Scanivalve pneumatic switch sequentially connected the pressure taps to a Barocet pressure transducer. Analog signals were sent through a 16-channel analog-to-digital converter to a 16-bit HP-1000 A700 minicomputer where the data were processed. Each pressure sample of a surface pressure tap extended over a time period corresponding to 140 rotor revolutions.

The unsteady component of the pressure was measured by the use of 18 microphone ports mounted flush with the airframe. Four microphone ports were available at any given time and additional measurement locations were obtained by moving the microphones from port to port as described in detail by Brand.[6] The microphones are about 3 mm in radius, and sampling of the signals was synchronized with a pulse from a rotor shaft encoder so that the azimuthally resolved data could be obtained.[6] The nominal spacing between the microphones is 38 mm. The microphone output signal was sampled at 1-deg increments of rotor azimuth and averaged over each 6-deg interval. The results at each 6-deg interval are then summed with similar data from 100 subsequent revolutions of the rotor. Details of the data reduction procedure are also given by Brand.[6]

Analysis

The calculation of the flowfield due to a generalized three-dimensional vortex in the presence of a cylinder is described in Part 1 of this study[2] for the case where the vortex is symmetric about the y axis; in what follows we discuss the specifics of the application of the theory to the experimental configuration. The physical situation is depicted in Fig. 1b; here (x,y,z) and (r,θ,z) denote Cartesian and polar coordinates with origin at the center of the cylindrical airframe. In general the flowfield consists of that induced by the vortex itself and that induced by the image field due to the vortex and to any other mean motion in which the vortex may be embedded. In the present work the mean streaming motion will satisfy the solid wall boundary condition at the cylinder surface, and so the problem reduces to calculating the effect of the image in the cylinder. The flow is assumed to be potential outside the vortex filament; thus the velocity field may be described by a velocity potential that satisfies $\nabla^2\phi' = 0$. Let $\phi' = \phi_I + \phi_V$ where ϕ_V is the potential due to a vortex in free space. Then ϕ_I satisfies

$$\nabla^2\phi_I = 0 \quad \text{with} \quad \frac{\partial\phi_I}{\partial r} = -\frac{\partial\phi_V}{\partial r} \quad \text{at} \quad r = 1 \tag{1}$$

and ϕ' must be bounded as $r^2 + z^2 \to \infty$. Here all lengths have been made dimensionless on the cylinder radius denoted by a, and ϕ' has been made dimensionless on $W_\infty a$ where W_∞ is the freestream velocity component along the airframe. Here $W_\infty = 10$ m/s for the advance ratio $\mu = 0.1$ and $W_\infty = 7.5$ m/s for $\mu = 0.075$. To obtain the solution to the boundary-value problem defined by Eq. (1) we use the Fourier transform in both the z and θ directions. Using the inversion formulas for the transforms as given in Churchill,[14] the solution to Eq. (1) is given by Eq. (4) of Part 1.[2]

The simplest way to model the effect of the downwash velocity on the vortex filament is to use the two-dimensional potential flow past a circular cylinder along with a constant velocity in the direction of the generators of the cylinder to simulate forward flight.[4,5] In the coordinate system of Fig. 1 this steady streaming motion, which is used for the mean flow in Part 1, may be written as

$$\boldsymbol{U}_M = \alpha\frac{\sin 2\theta}{r^2}\hat{i} - \alpha\left(1 + \frac{\cos 2\theta}{r^2}\right)\hat{j} + \hat{k} \tag{2}$$

where $\alpha = U_\infty/W_\infty$ is the ratio of the mean velocity at infinity in the y direction to the characteristic velocity W_∞, which is the mean streaming flow along the cylinder $r \to \infty$. Note that this mean distribution is symmetric with respect to the x direction, and thus the characteristic asymmetry of the motion of the tip vortex seen in experiments will not occur.

To better model the steady mean flow (both downwash and axial mean flow components), a model that captures the essential characteristics of the asymmetry of the vortex motion has been developed. The model consists of introducing the velocities $v(x)$ and $w(x)$, which are linear functions of x, to represent the undisturbed (i.e., not affected by the presence of the cylinder) and asymmetric mean flow in the y and z directions, respectively, in the region of rotor influence (note the rotor radius is about seven times that of the cylinder). It should be noted that the mean flow is modified only in the region underneath the rotor where the flow is not symmetric; outside this region, the mean flow is considered symmetric and corresponds to that described by Eq. (2). Thus, the undisturbed asymmetric mean flowfield is given by

$$\boldsymbol{U}_A = v(x)\hat{j} + w(x)\hat{k} \tag{3}$$

where

$$v(x) = Ax + B \tag{4}$$

$$w(x) = Cx + D \tag{5}$$

where A, B, C, and D are constants that are determined from the experimental conditions at the beginning of the computational

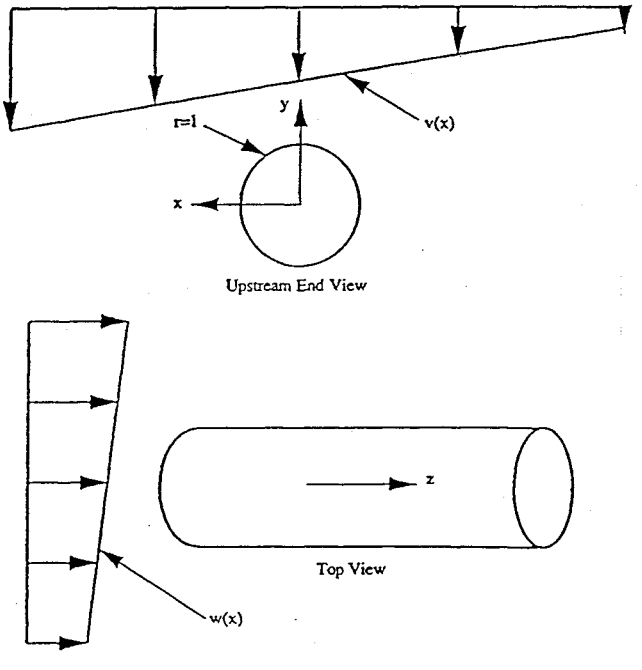

Fig. 3 Sketch of the mean flow viewed from upstream and the top of the cylinder. Note the linear profiles of the downwash $v(x)$ and the axial flow $w(x)$.

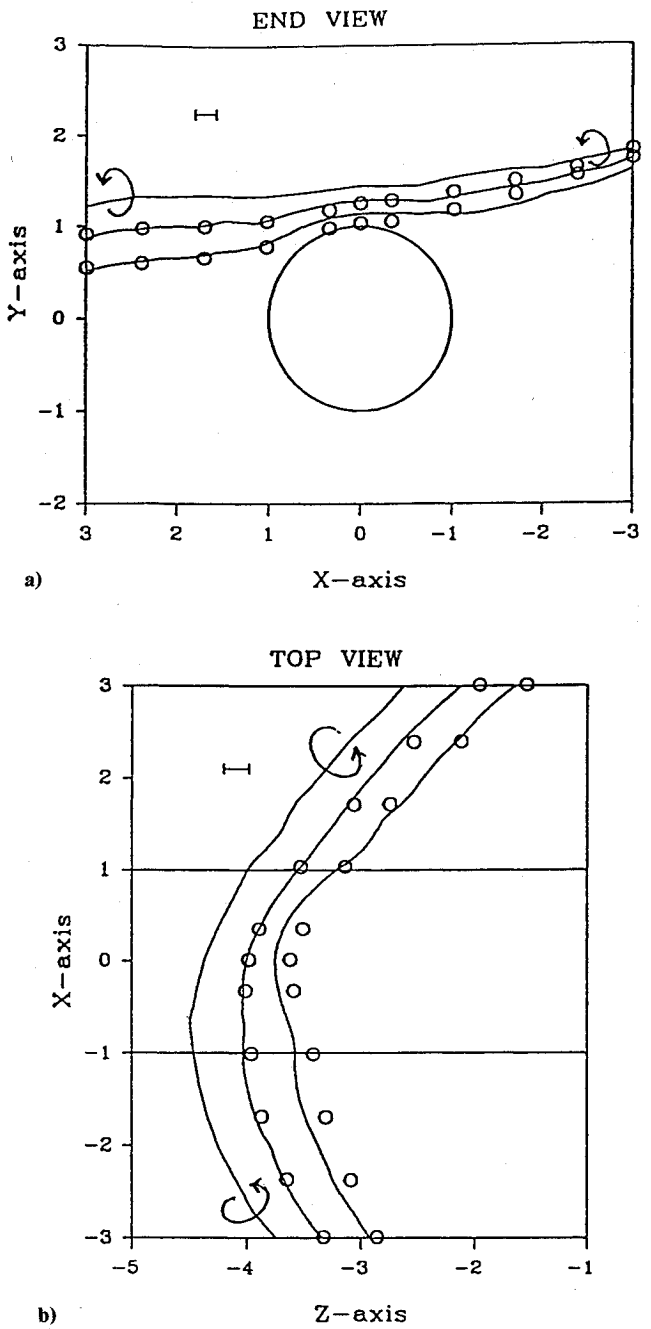

Fig. 4 Vortex trajectory for advance ratio $\mu = 0.1$: a) upstream end view and b) top view. The circles denote the experimental results (not to scale for the vortex core); the times shown are for $\psi = 0$ (the initial condition), 30, and 60 deg. The error bar in the experiments is also shown. The arrows indicate the sense of vortex circulation ($\Gamma > 0$).

time domain ($t = \psi = 0$). These constants are obtained by interpolating time-averaged experimental values measured at the endpoints of the vortex; these points are located at about three or four cylinder radii from the airframe, and their motion is most affected by the free streaming flow and the blade passage. Note that in the symmetric mean flow given by Eq. (2), which is used to describe the mean flow outside the region influenced by the rotor, the value of $\alpha = U_\infty/W_\infty$ is chosen to correspond to the value of B in Eq. (4). A physical estimate of U_∞ used in the present calculations for both advance ratios $\mu = 0.1$ and 0.075 will be given in the next section. The problem is depicted in Fig. 3 where the cylinder is immersed in a constant shear flow. Because the flow is assumed inviscid, the resulting vortical flowfield is preserved in time and no generation or dissipation of vorticity will occur. To find the asymmetric mean flow around the cylinder, we use the classical decomposition of a vector field into an irrotational component and a rotational one.[15,16] Thus, using this method, the asymmetric velocity field U_{AM} for the mean flow may be written as

$$U_{AM} = U_A + \nabla\Phi \tag{6}$$

where Φ is a scalar potential. Here

$$\nabla\Phi = v \tag{7}$$

is the velocity perturbation due to the presence of the cylinder. Equation (7) insures that the equation $\nabla \times v = 0$ is satisfied identically, and since the flow is assumed incompressible, Φ should satisfy

$$\nabla^2\Phi = 0 \tag{8}$$

Equation (8) is subject to the following boundary conditions:

$$\frac{\partial\Phi}{\partial r} = -v(x)\sin\theta \quad \text{at} \quad r = 1 \quad \text{and} \quad \Phi \text{ is finite as } r \to \infty \tag{9}$$

where $\partial\Phi/\partial r$ is the negative of the radial component of U_A and is given by

$$\frac{\partial\Phi}{\partial r} = -\frac{A}{2}r\sin 2\theta - B\sin\theta \tag{10}$$

Note that the constants C and D do not appear in Eq. (10), and thus the mean streaming motion along the axis is not affected by the presence of the cylinder. To obtain the solution to the boundary-value problem defined by Eqs. (8) and (9) we use finite Fourier transform in the θ direction. Defining the Fourier transform of Φ as

$$\hat{\Phi} = \int_{-\pi}^{\pi} \Phi e^{-im\theta}\, d\theta \tag{11}$$

the transform solution $\hat{\Phi}$ satisfies

$$\frac{\partial^2\hat{\Phi}}{\partial r^2} + \frac{1}{r}\frac{\partial\hat{\Phi}}{\partial r} - \frac{m^2}{r^2}\hat{\Phi} = 0 \tag{12}$$

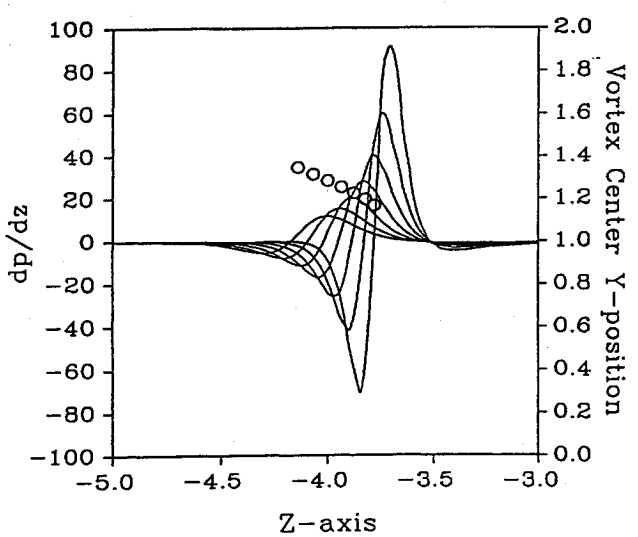

Fig. 5 Pressure gradient $\partial p/\partial z$ for $\mu = 0.1$ along the top of the airframe for several values of $\psi = 18$, 24, 30, 36, 42, 48, and 54 deg. The amplitude of the pressure gradient spike increases as ψ increases. The open circles are side views of the computed vortex head position.

After we apply the boundary conditions (9) in the transform space, a solution for $\hat{\Phi}$ is obtained

$$\hat{\Phi} = \begin{cases} \mp i\pi \dfrac{A}{2|m|} r^{-|m|}, & \text{for } m = \pm 2 \\ \mp i\pi \dfrac{B}{|m|} r^{-|m|}, & \text{for } m = \pm 1 \\ 0, & \text{otherwise} \end{cases} \tag{13}$$

Using the inversion formulas for the transform as given in Ref. 14, we may easily show that

$$\Phi(r, \theta) = \frac{A}{4} \frac{\sin 2\theta}{r^2} + B \frac{\sin \theta}{r} \tag{14}$$

Thus the resulting mean flow takes the form

$$\boldsymbol{U}_{AM} = (U_{AM_r} \cos\theta - U_{AM\theta} \sin\theta)\hat{i} + (U_{AM_r} \sin\theta + U_{AM\theta} \cos\theta)\hat{j} + w(x)\hat{k} \tag{15}$$

where U_{AM_r} and $U_{AM\theta}$ are, respectively, the radial and azimuthal components of the asymmetric mean flow and are given by

$$U_{AM_r} = \left[Ar \cos\theta \left(1 - \frac{1}{r^4}\right) + B\left(1 - \frac{1}{r^2}\right)\right] \sin\theta \tag{16}$$

and

$$U_{AM\theta} = -\frac{A}{2r^3} + \left[Ar \cos\theta \left(1 + \frac{1}{r^4}\right) + B\left(1 + \frac{1}{r^2}\right)\right] \cos\theta \tag{17}$$

To compute the self-induced motion of the filament, we adopt a cutoff procedure due originally to Moore[17] and refined by Hon and Walker.[18] In general the flow inside the vortex filament is assumed to be steady and to correspond to a two-dimensional Rankine vortex.

To advance the vortex filament, the induced velocity field on the filament is calculated; each point is then advanced according to the evolution equation

$$\frac{\partial \boldsymbol{X}}{\partial t}(s, t) = \boldsymbol{u} \tag{18}$$

where

$$\boldsymbol{X}(s, t) = [x(s, t), y(s, t), z(s, t)] \tag{19}$$

and the time scale t is defined by

$$t = \frac{W_\infty}{a} t^* \tag{20}$$

where t^* is dimensional. Note that the time is scaled differently from that of Part 1.[2] The total velocity field is thus given by

$$\boldsymbol{u} = \boldsymbol{U}_I + \boldsymbol{U}_V + \boldsymbol{U}_{AM} \tag{21}$$

where the velocity $\boldsymbol{u}$ has been nondimensionalized on W_∞ and

$$\boldsymbol{U}_V(\boldsymbol{X}, t) = -\frac{\Gamma}{4\pi} \int_C \frac{(\boldsymbol{X} - \boldsymbol{X}') \times d\boldsymbol{X}'}{|\boldsymbol{X} - \boldsymbol{X}'|^3} \tag{22}$$

where $\Gamma = \Gamma^*/W_\infty a$ is the dimensionless circulation.

The component $\boldsymbol{U}_I$ is the velocity field in the Cartesian system due to the image of the filament in the cylinder.[2] The evolution of the filament is computed by discretizing the filament and using a

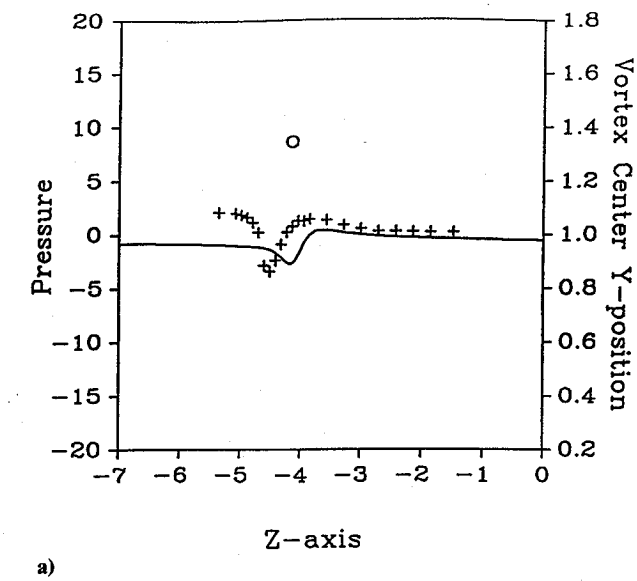

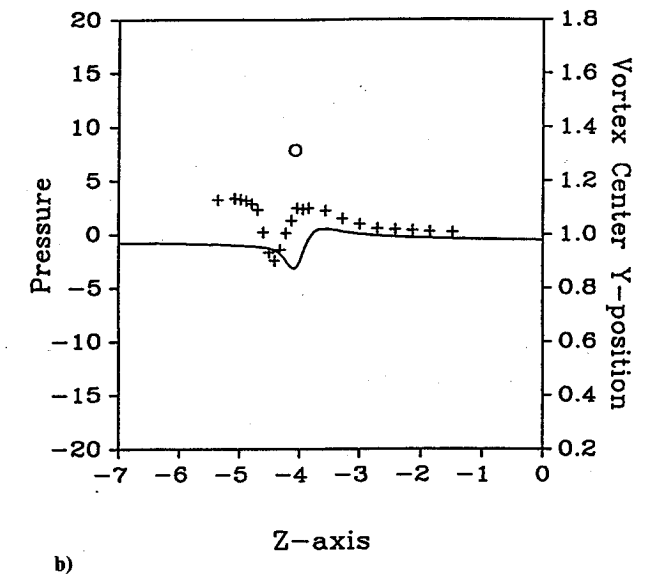

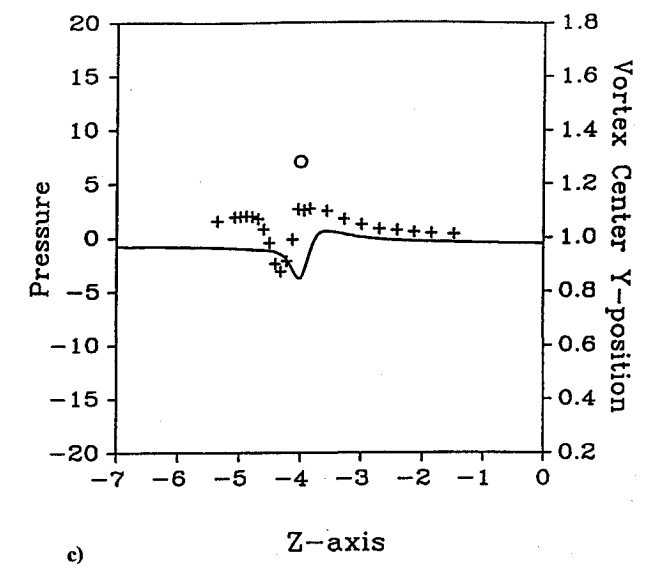

Fig. 6 Pressure distribution along the top of the airframe for several values of ψ for μ = 0.1. The circle is the side view of the computed vortex head position: a) ψ = 18 deg, b) ψ = 24 deg, and c) ψ = 30 deg.

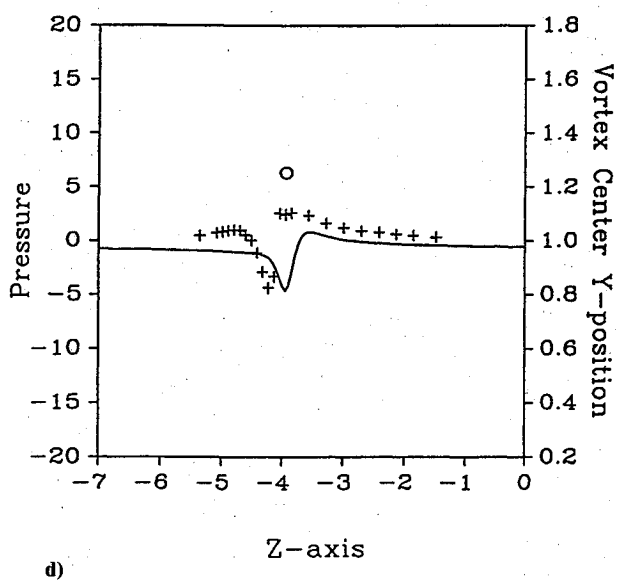

d)

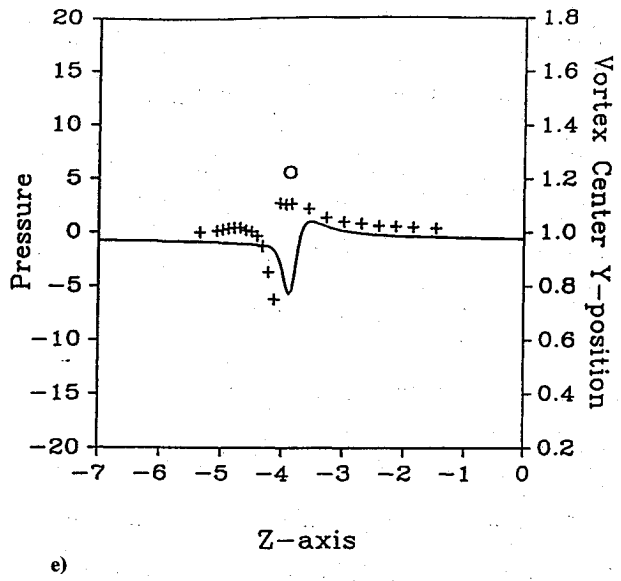

e)

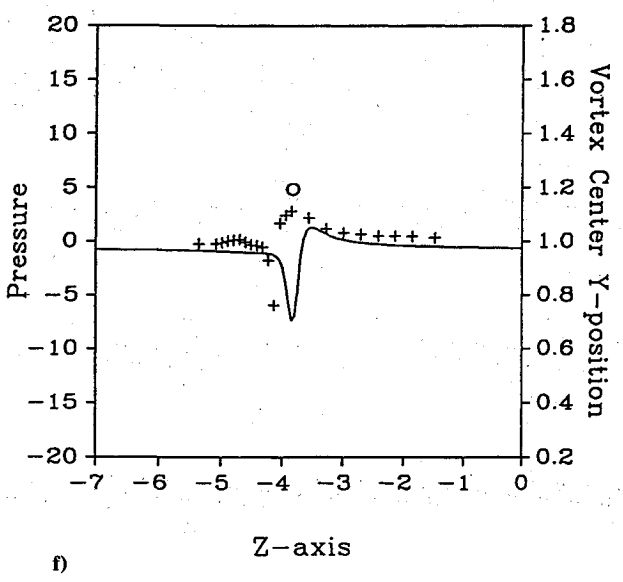

f)

fourth-order Runge-Kutta method in time; the integral appearing in the velocity field in Eq. (22) is evaluated using Simpson's rule, and the Fourier integrals involved in evaluating the image-induced velocity field at points off the vortex (on the surface of the cylinder) are computed using the fast Fourier transform procedure developed by Cooley and Tukey.[19] The pressure on the airframe is computed from Bernoulli's equation by

$$\frac{\partial \phi}{\partial t} + \frac{|u|^2}{2} + p = f_0(t) \tag{23}$$

where f_0 is the Bernoulli constant and p is the dimensionless pressure defined by

$$p = \frac{p^* - p_\infty}{1/2\,\rho W_\infty^2}$$

Experimental Conditions

There are a number of considerations involving the motion of the tip vortex filament in the experiments, and these issues are addressed in this section. In general, the initial position of the filament is given by

$$X(s, t=0) = x_s\hat{i} + y_s\hat{j} + z_s\hat{k} \tag{24}$$

In the present work the initial position of the vortex is specified by using the experimental data of Liou et al.[3] for $\mu = 0.1$ at $\psi = 0$; in this case there are 19 data points across the vortex. To better resolve the vortex filament these data points were used to interpolate once to obtain 37 points along the filament. The experimental data range from $x = -3.07$ to 3.07; to avoid a discontinuity in slope at each end of the filament, additional points were added so that the filament ends are assumed to be straight for $|x| > 5$. The parametric variable s ranges from -5 to 5 with the grid spacing in s, $\Delta s = 0.167$. For the case of $\mu = 0.075$, the experimental data set for the vortex position is not as extensive as that for $\mu = 0.1$. Consequently, the same initial condition was used for this case as that described earlier but was shifted to agree with the experimental centerline vortex position (i.e., from a side view) at $\psi = 0$. Because of the proximity of the vortex to the airframe, this procedure should be adequate to describe the subsequent vortex motion and instantaneous pressure distribution on the airframe.

The determination of the undisturbed and asymmetric mean downwash $v(x)$ that is given by Eq. (4) is more difficult. To esti-

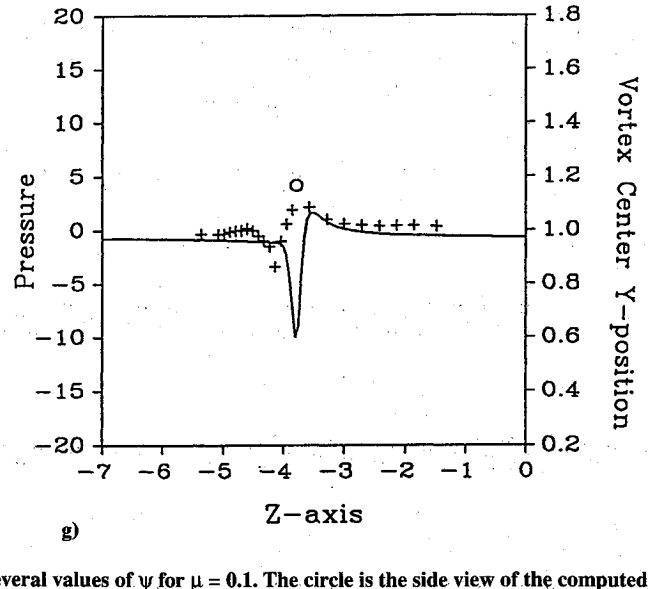

g)

Fig. 6 (Continued) Pressure distribution along the top of the airframe for several values of ψ for $\mu = 0.1$. The circle is the side view of the computed vortex head position: d) $\psi = 36$ deg, e) $\psi = 42$ deg, f) $\psi = 48$ deg, and g) $\psi = 54$ deg.

mate the downwash velocity in the experiments, the velocities of the vortex filament on the advancing and retreating sides of the rotor far from the cylinder (see Ref. 3, Fig. 3) are estimated using the data between the values of $\psi = 330$ and 540. The resulting downwash $v(x)$ is then obtained by linear interpolation. Using this procedure, the coefficients of $v(x)$ are approximated by $A = -0.208$ and $B = -0.557$ for the advance ratio $\mu = 0.1$. Since the magnitude of the dimensional downwash is kept the same for both advance ratios $\mu = 0.1$ and 0.075, the values of A and B for $\mu = 0.1$ are divided by 0.75 in the case $\mu = 0.075$. This results in a dimensional quantity $U_\infty = 5.57$ m/s, that is used to describe the symmetric mean flow [Eq. (2)] outside the region affected by the rotor.

The determination of the undisturbed asymmetric axial mean flow given by Eq. (5) is not trivial. From a fundamental point of view, the motion of the tip vortex is driven by the blade passage effect, by the balance of the rotor wake, by the image of the vortex in the airframe, and by its own self-induced motion. Consider the case of the advance ratio $\mu = 0.1$; direct calculation of the axial mean flow speed from the definition of the advance ratio yields $W_\infty \sim 10$ m/s, and this value was initially used in the calculations. Comparison of the position of the vortex filament at $\psi = 30$ and 60 deg with the experimental data revealed that the filament traveled significantly farther downstream than was evident in the calculations. To investigate this phenomenon, the velocity at the two ends of the vortex filament was estimated based on the results presented by Liou et al.[3] Because the ends of the filament are relatively far from the airframe, the ends should move at approximately the mean flow speed. The calculation revealed that the ends move somewhat faster than 10 m/s; moreover, each end of the filament travels at a different speed depending on whether it is on the retreating or advancing side of the rotor. Consequently, the resulting coefficients of $w(x)$ are estimated by $C = 0.045$ and $D = 1.315$. When this adjustment is made, the comparison with experiment is much better on the advancing side of the rotor as well as on the retreating side of the rotor.

The time scale of the motion may be calculated simply by using the definition of the angular speed of the rotor. For both values of the advance ratio, $\Delta\psi = 6$ deg corresponds to about 0.0476 s; in dimensionless form this corresponds to a value of $\Delta t = 0.0711$ for $\mu = 0.1$ and $\Delta t = 0.0533$ for $\mu = 0.075$. The accuracy of the solution for this value of the time step was checked by halving Δt for the case of $\mu = 0.1$ with no change in the computed results. The absolute value of the dimensional circulation has been estimated at 1.5 m^2/s.

The experimental work has suggested that significant axial flow is present in the core. However, since the azimuthal velocity within the core is much greater than the axial velocity, the incorporation of this effect into the calculations makes little difference in the results.[5] The assumed core size of the vortex is a key parameter. The core radius was measured from copper laser sheet flow visualization data and was found to range from 0.2 to 0.4 in. as the vortex approached the airframe; the increase in core radius is believed to be due to diffusion effects. For the calculations a mean radius equal to 0.3 in. was thus assumed. This results in a dimensionless core radius of about 0.11.

The pressure gradient has been calculated from the Euler equations and the pressure has been calculated from Bernoulli's equation. Calculation of the surface speeds requires the inversion of two Fourier transforms in the θ and z directions and the evaluation of an integral over the vortex filament.[2] The fast Fourier transform is employed for both transforms; 64 modes in the θ direction and 512 modes in the z direction have been used. The grid spacing in the z direction is $\Delta z = 0.05$, and so the computational spacing of the grid points corresponds to about one-half of a dimensionless vortex core radius. All of the grid parameters described in the pressure calculation have been tested for accuracy. The integral over the vortex filament is evaluated in the same manner as that employed in the calculation of the vortex position. However, because the velocities are more sensitive to numerical error than are the filament positions, it has been found necessary to use a much finer grid over the vortex filament; thus $\Delta s = 1/96$ in all of the pressure and pressure gradient calculations presented.

Results

As mentioned earlier, the evolution of the tip vortex filament and the induced pressure distribution on the airframe are of primary interest in the present study. The experimental results correspond to nominal advance ratios of 0.075 and 0.1. We consider the case of 0.1 first. Figure 4 shows the top and downstream end views of the vortex trajectory plotted at two subsequent times corresponding to $\psi = 30$ and 60 deg; the circles are the experimental data points. Here ψ is measured from the beginning of the period; in general, the absolute age of the vortex filament in the experiments is $\psi_{abs} = \psi + 360$ deg. The error bars correspond to about 15 mm, which is about one vortex diameter. Note the good agreement between theory and experiment, especially at $\psi = 30$ deg. At $\psi = 60$ deg the vortex is about to impact the airframe, and some uncertainty in the precise position of the filament near impact does exist; consequently, those experimental data points nearest the airframe should be viewed with caution. This is probably the reason for the rather substantial differences between the experiments and the computed results in the top view of the vortex position at $\psi = 60$ deg. Computational resolution of the vortex position has been maintained up to this time.

Figure 5 shows a typical pressure gradient $\partial p/\partial z$ induced on the airframe for $\mu = 0.1$ for several values of ψ; the computed side view of the vortex head position is represented by the open circles, which are not drawn to scale. Note the strong adverse pressure gradient that develops as the vortex approaches. Moreover, as ψ increases, the pressure gradient becomes more focused locally in space; in addition, it is apparent that a short time scale is emerging as evidenced by the rapid increase in the amplitude of the pressure gradient after $\psi = 42$ deg.

The pressure distribution along the top of the airframe is depicted in Fig. 6; each of the crosses corresponds to the experimental data points, and the open circle (not drawn to scale) denotes the side view of the computed vortex head position along the top of the airframe. For the smaller values of ψ, the effect of blade passage is rather substantial, as can be seen by the positive pressure values upstream of the vortex. As ψ increases, the effect of blade passage diminishes until, by $\psi = 48$ deg, the effect of the tip filament is dominant locally. Although the computed results slightly overpredict the experimental result in the later stages, the agreement is very good. Note the excellent agreement with the experimental data downstream of the vortex. The results show a shift in the position of the suction peak relative to the computed position of the vortex head; this may be due to uncertainty in the precise position of the vortex head in the experiments.

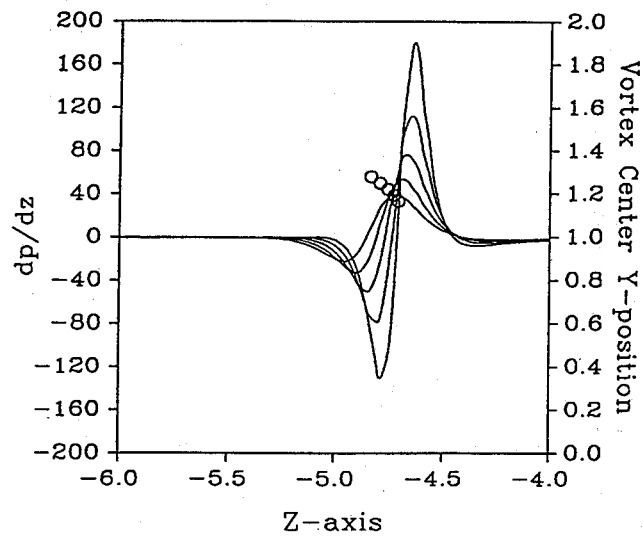

Fig. 7 Pressure gradient $\partial p/\partial z$ for $\mu = 0.075$ along the top of the airframe for several values of ψ = 18, 24, 30, 36, and 42 deg. The amplitude of the pressure gradient spike increases as ψ increases. The open circles are side views of the computed vortex head position.

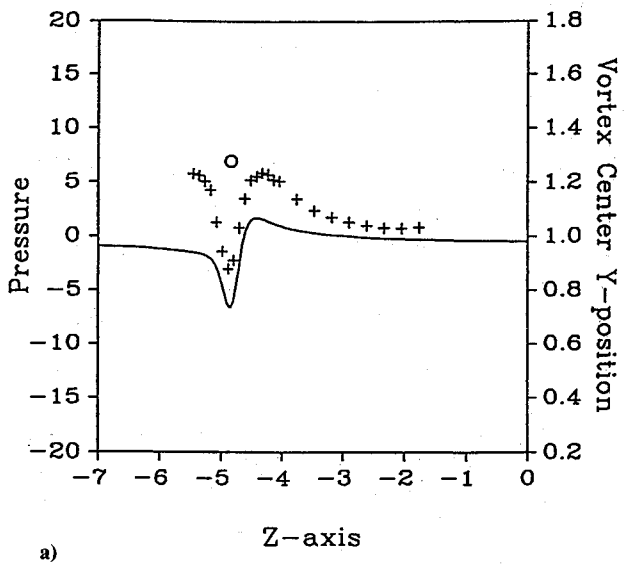

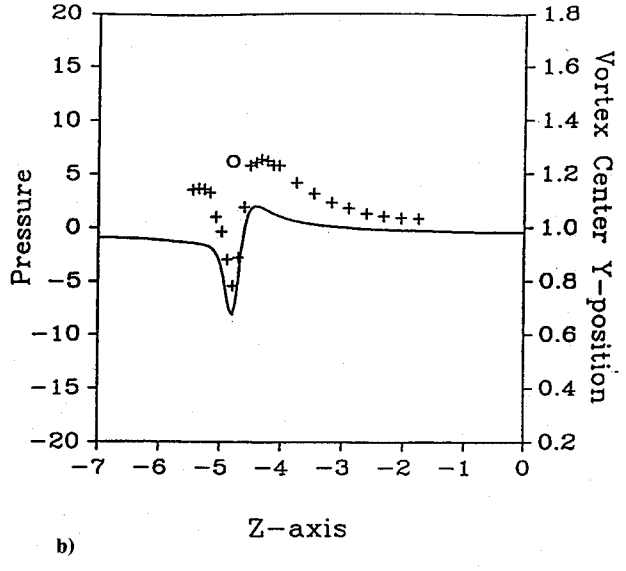

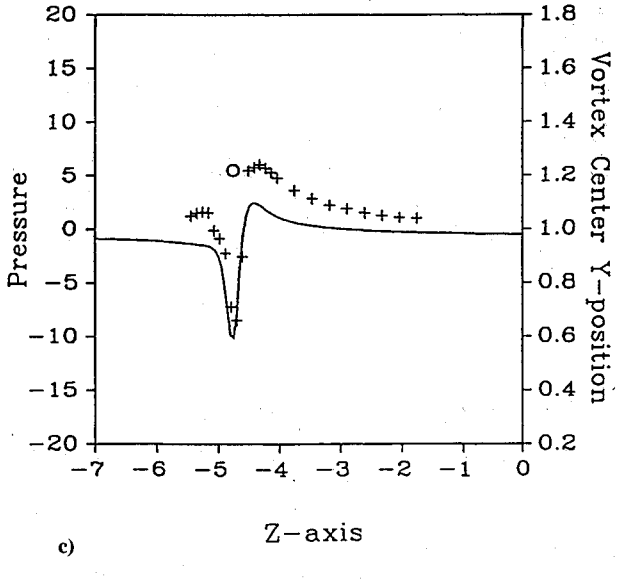

For the case of $\mu = 0.1$, other factors appear to influence the behavior of the pressure distribution at about $\psi = 54$ deg. One possibility, which is consistent with the visualization results,[3,4] is that the vortex core flow may be significantly affected by the presence of the airframe. This is manifest experimentally in a sudden decrease in the amplitude of the suction peak at this time, indicating possible destruction of the vortex core locally about the collision point. As mentioned in Part 1[2] of this study, the flow in the core of the vortex has been assumed to be of Rankine type and thus independent of time. Consequently, the present model cannot capture this behavior, thus establishing the approximate region of validity of the present model.

Figure 7 depicts the pressure gradient for the case of $\mu = 0.075$ for $\psi = 18$ to 42 deg in increments of 6 deg. These results are similar in form to the case of $\mu = 0.1$; however, it is apparent that in the later stages of the calculations the amplitude of the peak is higher. Figure 8 shows the corresponding results for the pressure. Results are shown for $\psi = 18$ to 42 deg in increments of 6 deg. As with the earlier results, the blade passage effect is evident at the lower values of ψ; as the vortex moves toward the airframe, the tip filament again becomes more dominant, and the present analytical/computational effort appears to adequately capture the phenomenon.

The contribution of the unsteady term $\partial\phi/\partial t$ to the pressure p appearing in Eq. (21) has also been investigated. The results from both cases of $\mu = 0.1$ and 0.075 show that $\partial\phi/\partial t$ accounts for a

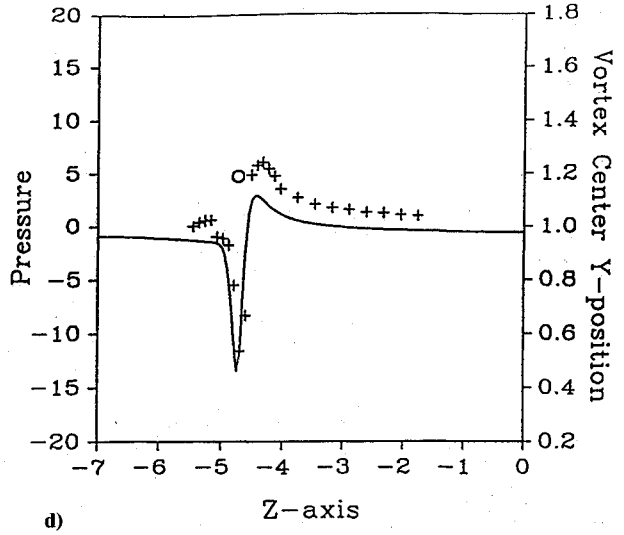

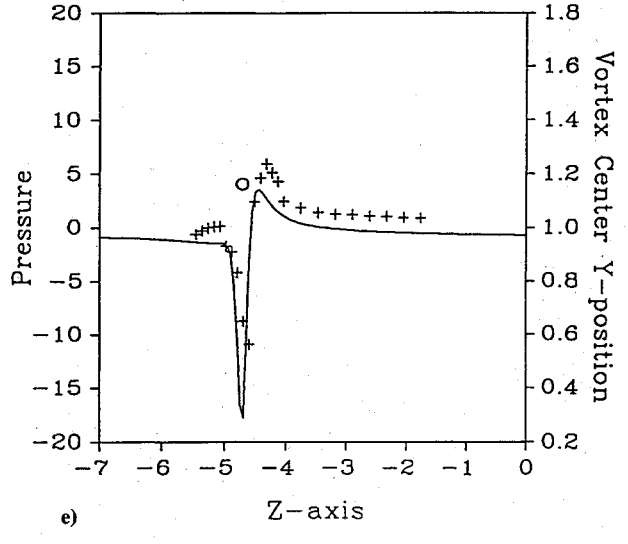

Fig. 8 Pressure distribution along the top of the airframe for several values of ψ for $\mu = 0.075$. The circle is the side view of the computed vortex head position: a) $\psi = 18$ deg, b) $\psi = 24$ deg, c) $\psi = 30$ deg, d) $\psi = 36$ deg, and e) $\psi = 42$ deg.

major part of the pressure during the initial stages from $\psi = 0$ to 30 deg. In the latter stages, $\partial\phi/\partial t$ has only a slight effect on the pressure suction peak; however, it remains the major factor in the growth of the positive pressure hump appearing downstream of the suction peak.

Summary

Experimental measurements of the strong interaction of a tip vortex with a cylindrical airframe have been performed, and the results have been compared with the results of a simplified model for this interaction. Results have been presented for the vortex path and the pressure distribution for two advance ratios indicative of low-speed forward flight. The experimental and analytical/numerical results are in substantial agreement for both the pressure and the vortex path during the time period before vortex impact. Although some of the experimental data have been employed to determine the mean flow speed far from the airframe, the present analytical/computational effort is substantially free of fit parameters and may thus be termed a predictive effort. Estimates for the initial position of the vortex, the circulation of the vortex, and the vortex core radius have been determined directly from the experiments. In particular, it has been shown that the position and magnitude of the suction peak induced on the airframe can be adequately predicted using a three-dimensional potential flow analysis during the time period from the onset of strong interaction with the airframe until just before the vortex-airframe collision.

The development of a very strong suction peak coincides with the emergence of a very large adverse pressure gradient, a feature that is often responsible for initiating boundary-layer separation. Additional computational effort is underway to push the calculations further into the collision process, and the computation of the boundary-layer flow on the airframe is currently under investigation.

The question of the characteristics of the initial stages of vortex impact can now be addressed. A videotape of the experiments of Liou et al.[3] and Brand[6] indicates (from the side view) that the vortex core undergoes a rapid deformation as the airframe is approached. In particular, it is noted that a local rapid flattening of the smoke patterns that define the boundary of the vortex core takes place just before impact with the cylinder. This phenomenon had also been observed earlier by Simons et al.[20] Investigation of the videotape results indicates that this rapid flattening apparently begins when the vortex is still outside the boundary layer, and during this period, a large change in the time evolution of filament curvature at points removed from the immediate neighborhood of the collision does not appear to occur.[3] This observation suggests that the deformation of the vortex core structure is essentially a local phenomenon. It is difficult to quantify the time scale of this vortex core deformation; however, the present numerical results indicate that the time scale is much faster than the time scale of the vortex evolution process and is probably related to the dimension of the vortex core.

Acknowledgments

The experiments, analysis, and computational work have been supported by the U.S. Army Research Office under contracts DAAL03-K-0095 (analysis) and DAAL03-88-C-0003 (experiments). The continued support of the contract monitor, Thomas L. Doligalski, is greatly appreciated. The computations have been performed through a grant of computer time from the Ohio Supercomputer Center.

References

[1]Sheridan, P. F., and Smith, R. F., "Interactional Aerodynamics—A New Challenge to Helicopter Technology," *Journal of the American Helicopter Society*, Vol. 25, No. 1, 1980, pp. 3–21.

[2]Affes, H., and Conlisk, A. T., "Model for Rotor Tip Vortex-Airframe Interaction, Part 1: Theory," *AIAA Journal*, Vol. 31, No. 12, 1993, pp. 2263–2273; also AIAA Paper 92-0320, 1992.

[3]Liou, S. G., Komerath, N. M., and McMahon, H. M., "Measurement of the Interaction Between a Rotor Tip Vortex and a Cylinder," *AIAA Journal*, Vol. 28, No. 6, 1990, pp. 975–981.

[4]Brand, A. G., McMahon, H. M., and Komerath, N. M., "Correlations of Rotor/Wake-Airframe Interaction Measurements with Flow Visualization Data," *Proceedings of the 46th Annual Forum of the American Helicopter Society* (Washington, DC), American Helicopter Society, Alexandria, VA, Vol. 2, 1990, pp. 1135–1143.

[5]Affes, H. and Conlisk, A. T., "The Unsteady Interaction of a Three-Dimensional Vortex Filament With a Cylinder," *Proceedings of the International Specialists' Meeting on Rotorcraft Basic Research*, Georgia Inst. of Tech., Atlanta, GA, March 25–27, 1991, pp. 37-1–37-11.

[6]Brand, A. G., "An Experimental Investigation of the Interaction Between a Model Rotor and Airframe in Forward Flight," Ph.D. Thesis, Dept. of Aerospace Engineering, Georgia Inst. of Tech., Atlanta, GA, 1989.

[7]Bi, N.-P., and Leishman, J. G., "Experimental Study of Rotor/Body Aerodynamic Interactions," *Journal of Aircraft*, Vol. 27, No. 9, 1990, pp. 779–788.

[8]Bi, N.-P., and Leishman, J. G., "Analysis of Unsteady Pressures Induced on a Body in the Vicinity of a Rotor," *Proceedings of the International Specialists' Meeting on Rotorcraft Basic Research*, Georgia Inst. of Tech., Atlanta, GA, March 25–27, 1991, pp. 38-1–38-20.

[9]Leishman, J. G., and Bi, N.-P., "Aerodynamic Interactions Between a Rotor and a Fuselage in Forward Flight," *Journal of the American Helicopter Society*, Vol. 35, No. 3, 1990, pp. 22–31.

[10]Lorber, P. F., and Egolf, T. A., "An Unsteady Helicopter Rotor-Fuselage Aerodynamic Interaction Analysis," *Journal of the American Helicopter Society*, Vol. 36, No. 3, 1990, pp. 32–42; see also NASA Rept. 4178, Sept. 1988.

[11]Mavris, D. M., Komerath, N. M., and McMahon, H. M., "Prediction of Aerodynamic Rotor-Airframe Interactions in Forward Flight," *Journal of the American Helicopter Society*, Vol. 34, No. 4, 1989, pp. 37–46.

[12]Quakenbush, T. R., and Bliss, D. B., "Vortex Methods for the Computational Analysis of Rotor/Body Interaction," *Proceedings of the 48th Annual Forum of the American Helicopter Society* (Washington, DC), American Helicopter Society, Alexandria, VA, June 1992, pp. 475–488.

[13]Komerath, N. M., Mavris, D. M., and Liou, S.-G., "Prediction of Unsteady Pressure and Velocity over a Rotorcraft in Forward Flight," *Journal of Aircraft*, Vol. 28, No. 8, 1991, pp. 509–516.

[14]Churchill, R. V., *Operational Mathematics*, 3rd ed., McGraw-Hill, New York, 1972, pp. 379, 471.

[15]Lamb, H., *Hydrodynamics*, 6th ed., Cambridge Univ. Press, Cambridge, England, UK, 1932.

[16]Richardson, S. M, and Cornish, A. R. H., "Solution of Three-Dimensional Incompressible Flow Problems," *Journal of Fluid Mechanics*, Vol. 82, 1977, pp. 309–319.

[17]Moore, D. W., "Finite Amplitude Waves on Aircraft Trailing Vortices," *Aeronautical Quarterly*, Vol. 23, Part 4, 1972, pp. 307–314.

[18]Hon, L. and Walker, J. D. A., "An Analysis of the Motion and Effects of Hairpin Vortices," Dept. of Mechanical Engineering and Mechanics , Lehigh Univ., Rept. FM-11, Bethlehem, PA, Aug. 1987.

[19]Cooley, J. W., and Tukey J. W., *Mathematics of Computation* , Vol. 19, 1965, pp. 297–301.

[20]Simons, I. A., Pacifico R. R., and Jones, J. P., "The Movement, Structure, and Breakdown of Trailing Vortices from a Rotor Blade," *Proceedings of the CAL/USAA AVLABS Symposium*, Buffalo, NY, 1966.